*J. Fluid Mech.* (2006), *vol.* 562, *pp.* 303–312. © 2006 Cambridge University Press 
doi:10.1017/S0022112006001388 Printed in the United Kingdom

# Axisymmetric breakup of bubbles at high Reynolds numbers

By J. M. GORDILLO AND M. PÉREZ-SABORID

Área de Mecánica de Fluidos, Universidad de Sevilla. Avda. de los Descubrimientos s/n, 41092, Sevilla, Spain
jgordill@us.es

(Received 31 January 2006 and in revised form 13 June 2006)

We have analysed the structure of the irrotational flow near the minimum radius of an axisymmetric bubble at the final instants before pinch-off. The neglect of gas inertia leads to the geometry of the liquid–gas interface near the point of minimum radius being slender and symmetric with respect to the plane $z=0$. The results reproduce our previous finding that the asymptotic time evolution for the minimum radius, $R_o(t)$, is $\tau \propto R_o^2\sqrt{-\ln R_o^2}$, $\tau$ being the time to breakup, and that the interface is locally described, for times sufficiently close to pinch-off, by $f(z,t)/R_o(t) = 1-(6\ln R_o)^{-1}(z/R_o)^2$. These asymptotic solutions correspond to the attractor of a system of ordinary differential equations governing the flow during the final stages before pinch-off. However, we find that, depending on initial conditions, the solution converges to the attractor so slowly (with a logarithmic behaviour) that the universal laws given above may hold only for times so close to the singularity that they might not be experimentally observed.

## 1. Introduction

Unlike the capillary-driven breakup of drops or liquid threads in a gas environment and the viscous breakup of a bubble, which have been precisely described and experimentally verified (Eggers 1993; Chen & Steen 1997; Day, Hinch & Lister 1998; Chen, Notz & Basaran 2002; Doshi *et al.* 2003; Suryo, Doshi & Basaran 2004; Burton, Waldrep & Taborek 2005), the description and measurement of the final stages before pinch-off of axisymmetric bubbles at high Reynolds numbers is still an open problem that has recently aroused great interest. A main difference between bubble and drop pinch-off at high Reynolds numbers is that the final instants of the former are driven either by liquid inertia or by a balance between gas and liquid inertia and not by capillary forces as is the case for drop breakup in air (Chen & Steen 1997; Day *et al.* 1998; Leppinen & Lister 2003). Indeed, inviscid bubble breakup is a process which can be driven solely by liquid inertia if the gas pressure drop through the bubble minimum radius is negligible. In this case, bubble breakup is slender and symmetric (Burton *et al.* 2005; Gordillo *et al.* 2005; Rodríguez-Rodríguez, Gordillo & Martínez-Bazán 2006; Bergmann *et al.* 2006; Leppinen, Lister & Eggers 2005) whereas, if gas inertia becomes of the order of the liquid inertia, breakup is non-slender and asymmetric (Gordillo *et al.* 2005).

The first analytical description of the time evolution of the bubble minimum radius was provided by Longuet-Higgins, Kerman & Lunde (1991) using a continuity argument, and by Oguz & Prosperetti (1993), who made use of the cylindrical

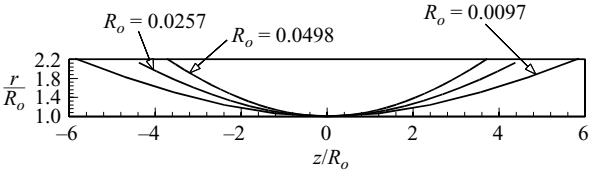


FIGURE 1. Time evolution of the bubble interface near the minimum radius, showing that bubble breakup is slender. The simulation has been performed with the boundary integral numerical code described in Rodríguez-Rodríguez *et al.* (2006).

(or two-dimensional) Rayleigh equation. In both contributions the liquid convective acceleration was neglected compared to the local one and the authors concluded that the bubble minimum radius approaches the singularity as $R_o \propto \tau^{1/2}$, with $R_o$ and $\tau$ the dimensionless minimum radius and time to singularity respectively. However, as shown in Gordillo *et al.* (2005), the effect of liquid convective terms is to slow down the breakup process or, equivalently, that the exponent in the power law for the minimum radius to be larger than 1/2. More precisely, the analysis retaining convective terms yields a time evolution of the form $\tau \propto R_o^2\sqrt{-\log R_o^2}$, which introduces a logarithmic correction to that found by the previous authors. An exponent in the power law larger than 1/2 was also experimentally and numerically reported by Bergmann *et al.* (2006) and numerically by Leppinen *et al.* (2005).

We have extended the analysis for the case of negligible gas inertia presented in Gordillo *et al.* (2005) in order to describe the time evolution of both the bubble minimum radius and the radius of curvature of the interface. Figure 1 shows the time evolution of the bubble interface near the minimum radius and close to the time the bubble pinches off under conditions in which gas inertia is negligible. Consistently with what was stated above, breakup is slender and symmetric. We have analysed the structure of the flow near the minimum radius assuming that: (i) breakup is axisymmetric, (ii) the flow is irrotational, (iii) liquid inertia dominates over surface tension and (iv) gas inertia can be neglected. Regarding liquid viscosity, our analysis will be valid if the initial Reynolds number satisfies $Re_c = \rho_l u_c a_c/\mu \gg 1$, $\mu$ and $\rho_l$ being, respectively, the liquid viscosity and liquid density and $a_c$ and $u_c$ the characteristic *initial* values of the radius of the bubble and liquid velocity, respectively. If the local Reynolds number is large, surface tension will be irrelevant describing the final instants before pinch-off, independently of the characteristic *initial* value of the Weber number, namely, $We_c = \rho_l u_c^2 a_c/\sigma$, with $\sigma$ the surface tension. In effect, note that, since $\tau = t_b - t \propto R_o^2\sqrt{-\log R_o^2}$, with $t_b$ the time to breakup, radial liquid velocity is of the order of $u_c\dot{R}_o \propto u_c/(R_o\sqrt{-\log R_o^2})$, with $\dot{R}_o = \mathrm{d}R_o/\mathrm{d}\tau$. Consequently, the ratio of viscous stress $\sim \mu u_c\dot{R}_o/(a_c R_o)$ to liquid inertia $\sim \rho_l u_c^2(\dot{R}_o)^2$, yields $\mu/(\rho_l u_c a_c \dot{R}_o R_o) = Re_c^{-1}\sqrt{-\ln(R_o)}$ and the ratio of pressure drop across the interface $\sim \sigma/(a_c R_o)$ to liquid inertia yields $We_c^{-1}[-R_o\ln(R_o)] \to 0$ for $R_o \to 0$. This latter estimate indicates that surface tension effects can be safely neglected in the analysis provided that the local Reynolds number $[Re_c^{-1}\sqrt{-\ln(R_o)}]$ is large. This condition is always satisfied if $Re_c \gg 1$ as $R_o < 10^{-30}$ in order for $\sqrt{-\ln(R_o)} \sim O(10)$. Note that $Re_c \gg 1$ is commonly satisfied in the usual case of bubble breakup in water. Indeed, the minimum value of the Reynolds number of the flow to break up a gas bubble in water is $Re_c > 250$ for the typical values of water viscosity $\mu = 10^{-3}\,\mathrm{kg\,m^{-1}\,s^{-1}}$, air-water surface tension $\sigma = 7\times10^{-2}\,\mathrm{N\,m^{-1}}$, $a_c = 10^{-3}\,\mathrm{m}$, and the minimum characteristic liquid velocity to breakup the bubble, which can be estimated to be $u_c \gtrsim [\sigma/\rho_l a_c]^{1/2}$

(this estimate can be deduced from the fact that $We_c \gtrsim O(1)$ is a necessary condition to breakup the bubble, as pointed out in Rodríguez-Rodríguez *et al.* 2006). As shown in Revuelta, Rodriguez-Rodriguez & Martinez-Bazan (2006), $Re_c = 250$ is sufficiently large for viscous effects to be neglected in a first approach and therefore, many common bubble breakup events take place at high Reynolds numbers (for experimental evidence see, for instance, Rodríguez-Rodríguez *et al.* 2006; Bergmann *et al.* 2006). Furthermore, our analysis will be valid if during the breakup process, gas inertia is negligible compared with liquid inertia, namely, $\rho_g[Q_g/(a_c R_o)^2]^2 \ll \rho_l u_c^2(\dot{R}_o)^2$, with $\rho_g$ and $Q_g$ the gas density and gas flow rate trough the minimum radius. Otherwise bubble breakup will be non-slender and asymmetric (see Gordillo *et al.* 2005). Finally, note that our results will be valid to describe the final 1 %–0.1 % of the total time evolution of the bubble interface; this means that, for the typical values provided above, our analysis will cover the final 100 μs–10 μs of the breakup process.

## 2. Analysis of the irrotational flow near the minimum radius

In this section we analyse the final stages of the breakup process of an axisymmetric gas bubble enclosed by an infinite volume of an incompressible and inviscid liquid. For simplicity, the density of the gas within the bubble will be assumed negligible compared to that of the liquid so that the motion of the latter will not be affected by the former. The irrotational, axisymmetric flow of the liquid surrounding the bubble is governed by the Laplace and Bernoulli equations for the velocity potential, $\phi$, and the pressure, $p$, respectively,

$$\nabla^2\phi = (1/r)(r\phi_r)_r + \phi_{zz} = 0, \tag{2.1}$$

$$\frac{\partial\phi}{\partial t} + \frac{|\nabla\phi|^2}{2} + p = P, \tag{2.2}$$

where subscripts $r$ and $z$ denote partial derivatives with respect to the radial and axial coordinates respectively. In (2.1) and (2.2) all quantities have been made dimensionless using the liquid density, $\rho_l$, and the characteristic initial radius of the bubble and liquid velocity, $a_c$ and $u_c$ respectively; the term $P$ in (2.2) depends only on time and can be set equal to zero (by redefining $\phi$) without affecting the velocity field. Equations (2.1) and (2.2) must be solved together with the equation governing the motion of the free surface (gas–liquid interface), $r = f(z, t)$,

$$\frac{\partial F}{\partial t} + \boldsymbol{v}\cdot\nabla F = 0, \tag{2.3}$$

where $F = r - f(z, t)$. As justified above, the capillary pressure jump across the interface can be neglected in the analysis and, consequently, equation (2.2) simplifies to

$$\frac{\partial\phi}{\partial t} + \frac{|\nabla\phi|^2}{2} = 0. \tag{2.4}$$

In order to solve (2.1) and (2.3) first note that, since the bubble is symmetric respect to the plane $z = 0$, in a sufficiently small region near the minimum radius, $R_o(t)$, both the free surface and the local potential can be expanded in even powers of $z$ as

$$f(z, t) = R_o(t) + r_1(t)z^2 + O(z^4), \tag{2.5}$$

$$\phi(r, z, t) = \Phi(r, t) + (r\varphi_r)_{rr}z^2/2 + O(z^4), \tag{2.6}$$

where $\Phi(r, t)$, $\varphi(r, t)$, $R_o(t)$ and $r_1(t)$ are unknown functions, the determination of which yields the solution of the problem; note that $r_1$ represents the curvature (inverse

of the radius of curvature) at the point of minimum radius. If (2.6) is introduced into (2.1) and terms of order $z^2$ are neglected one obtains a differential equation in $r$ which can be readily integrated to give

$$\Phi = A(t)\ln r - r\varphi_r + \varphi, \tag{2.7}$$

where $A(t)$ is an unknown function of time. On the other hand, substitution of (2.6) and (2.5) in (2.3) yields

$$-\left(\frac{\mathrm{d}R_o}{\mathrm{d}t} + \frac{\mathrm{d}r_1}{\mathrm{d}t}z^2\right) + [\Phi_r + (r\varphi_r)_{rrr}z^2/2 - 2r_1(r\varphi_r)_{rr}z^2]_{r=R_o+r_1z^2} = 0. \tag{2.8}$$

Note that it is always possible to find a region sufficiently close to the point of minimum radius ($r = R_o(t), z = 0$) where the axial distances satisfy the relation $r_1 z^2 \ll R_o$. Therefore, we can linearize the second term in (2.8) around $r = R_o$ and equate terms in powers of $z^0$ and $z^2$ in the resulting expression, which yields the equations

$$\frac{\mathrm{d}R_o}{\mathrm{d}t} = \frac{A}{R_o} - R_o\varphi_{rr}(R_o), \tag{2.9}$$

$$\frac{\mathrm{d}r_1}{\mathrm{d}t} = \left[-\frac{A}{R_o^2} - (r\varphi_{rr})_r(R_o)\right]r_1 + \frac{1}{2}(r\varphi_r)_{rrr}(R_o) - 2r_1(r\varphi_r)_{rr}(R_o). \tag{2.10}$$

Equations (2.9) and (2.10) relate the unknowns $A$ and $\varphi$ defining the potential with those defining the free surface, namely, $R_o$ and $r_1$. Another two relations between the unknowns are obtained from Bernoulli's equation evaluated at the free surface (2.5). In effect, substitution of (2.6) into (2.4) yields the equation

$$\left[\ln r\frac{\mathrm{d}A}{\mathrm{d}t} + \frac{\partial}{\partial t}(\varphi - r\varphi_r) + \frac{z^2}{2}\frac{\partial}{\partial t}(r\varphi_r)_{rr} + \frac{1}{2}\Phi_r^2 + \frac{z^2}{2}[\Phi_r(r\varphi_r)_{rrr} + [(r\varphi_r)_{rr}]^2]\right]_{r=R_o+r_1z^2} = 0. \tag{2.11}$$

which, after linearizing around $R_o$ and equating terms in powers of $z^0$ and $z^2$, gives

$$\ln R_o\frac{\mathrm{d}A}{\mathrm{d}t} + \left[\frac{\partial\varphi}{\partial t} - R_o\frac{\partial\varphi_r}{\partial t} + \frac{1}{2}\left(\frac{A}{R_o}\right)^2 + \frac{1}{2}[R_o\varphi_{rr}]^2 - A\varphi_{rr}\right]_{r=R_o} = 0, \tag{2.12}$$

$$\frac{r_1}{R_o}\frac{\mathrm{d}A}{\mathrm{d}t} + \left[r_1\frac{\partial\varphi_r}{\partial t} - r_1\frac{\partial}{\partial t}[(r\varphi_r)_r] + \frac{1}{2}\frac{\partial}{\partial t}[(r\varphi_r)_{rr}] + r_1[\Phi_r\Phi_{rr}] + \frac{1}{2}\left\{[\Phi_r(r\varphi_r)_{rrr}] + [r\varphi_r]_{rr}^2\right\}\right]_{r=R_o} = 0. \tag{2.13}$$

Note that (2.9)–(2.10) and (2.12)–(2.13) constitute a system of four equations for the unknowns $R_o(t)$, $r_1(t)$, $A(t)$ and $\varphi$ together with its temporal and radial derivatives. Therefore, to close the problem we need to know the functional dependence of $\varphi$ on $r$ and $t$. This will be achieved by matching the solution (2.6)–(2.7) of Laplace's equation valid in the region ($r \sim R_o$, $r_1 z_{end}^2 \ll R_o$), which will be called the inner solution, with an outer solution valid in a region such that $r \gg R_o$ and $r \ll z_{end}$, where $z_{end}$ is a value of the axial coordinate such that points with $z > z_{end}$ have a negligible influence on the potential at the point $(r, z)$. The conditions defining the outer region can both be satisfied due to the slenderness assumption; in that region the potential at the

plane $z=0$ is approximately that corresponding to the superposition of a continuous distribution of sources and dipoles along the bubble axis, namely

$$\phi(r, z=0) = 2\int_0^{z_{end}} \frac{Q_0(t)+Q_2 z'^2}{\sqrt{r^2+z'^2}}\,\mathrm{d}z' + 2\int_0^{z_{end}} \frac{D_1(t)z'^2 + D_3 z'^4}{(r^2+z'^2)^{3/2}}\,\mathrm{d}z'. \tag{2.14}$$

The integrations in (2.14) can be carried out analytically and, in the limit $r/z_{end} \ll 1$, they provide at leading order

$$\phi(r, z=0) = C + A(t)\ln r + B(t) r^2 \ln r + O(r^2) \tag{2.15}$$

where $C$ is a constant. Thus, the matching of expressions (2.15) and (2.7) yields $\varphi$ as

$$\varphi - r\varphi_r = B(t) r^2 \ln r \rightarrow \varphi = B(t) r^2 (1 - \ln r), \tag{2.16}$$

and the functional form of the potential in the inner region now becomes completely determined by (2.6) as

$$\phi = A(t)\ln r + B r^2 \ln r - 2z^2 B(1+\ln r). \tag{2.17}$$

Inserting (2.16)–(2.17) into (2.9)–(2.10) we obtain, after some algebra,

$$A = p + q, \quad B = -\frac{q}{R_o^2(1+2\ln R_o)}, \tag{2.18}$$

with

$$p = R_o \frac{\mathrm{d}R_o}{\mathrm{d}t}, \quad q = -R_o^2 \frac{2\ln R_o + 1}{-2 + 12(1+\ln R_o) R_o r_1} \frac{\mathrm{d}(R_o r_1)}{\mathrm{d}t}. \tag{2.19}$$

The equations for $p$ and $q$ can now be readily obtained by using (2.16)–(2.17) and (2.18)–(2.19) in (2.12)–(2.13) which yields, in terms of $s = -\ln R_o$ and the dependent variables $\ln p$ and $v = q/p$:

$$s\frac{\mathrm{d}\ln p}{\mathrm{d}s}\left(1 + s\frac{R_o r_1}{1-s}\right) + \left(\frac{1}{2} + s^2\frac{R_o r_1}{1-s}\right) + \frac{2s}{1-s}\left(s - \frac{2(1-s)}{1-2s}\right)v - \frac{8v^2 s^2(1-s)}{(1-2s)^2} = 0, \tag{2.20}$$

$$\begin{aligned} s\left(1 + s\frac{R_o r_1}{1-s}\right)\frac{\mathrm{d}v}{\mathrm{d}s} = {} & \left(v + \frac{R_o r_1}{2}\frac{1-2s}{1-s}\right)\left(\frac{1}{2} + s^2\frac{R_o r_1}{1-s} + \frac{2s}{1-s}\left[s - \frac{2(1-s)}{1-2s}\right]v\right. \\ & \left. - \frac{8v^2 s^2(1-s)}{(1-2s)^2}\right) + s\left(1 + s\frac{R_o r_1}{1-s}\right)\left(-\frac{R_o r_1}{2}\frac{1-2s}{1-s} - \frac{v}{1-s}\right. \\ & \left. \times \left(2(1-s) + \frac{1}{1-2s}\right) + \frac{4v^2(1-s)}{1-2s}\right). \end{aligned} \tag{2.21}$$

Note that equations (2.20)–(2.21), together with the pair of equations (2.19) defining $p$ and $q$, which can be written as

$$\frac{\mathrm{d}(R_o r_1)}{\mathrm{d}s} = \frac{v[-2 + 12 R_o r_1(1-s)]}{1-2s}, \tag{2.22}$$

$$\frac{\mathrm{d}t}{\mathrm{d}s} = -\frac{\exp(-2s)}{p}, \tag{2.23}$$

form a system of four equations for $p$, $v$, $R_o r_1$ and $t$ as functions of $s = -\ln R_o$; also note that equations (2.21)–(2.22) are decoupled from (2.20) and (2.23). System (2.20)–(2.23) can be readily integrated numerically once appropriate initial conditions

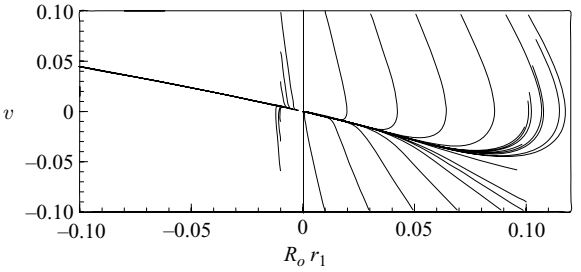


FIGURE 2. Different trajectories in the $v-R_o r_1$ plane resulting from the integration of equations (2.24)–(2.25) for $s_0 = 6$. Note that all trajectories tend to the line $v = -(1/2)\, R_o r_1$ for sufficiently large values of $s$. If initially $R_o r_1 > 0$ solutions tend to $R_o r_1 = 0$, thus becoming more slender. However, if initially $R_o r_1 < 0$ bubble breakup is no longer slender. This is a general trend, independent of the initial value of $s$.

are provided. However, since we are interested in the description of the final instants before pinch-off ($R_o \to 0$) it is worthwhile to look first at the behaviour of the solutions for large values of $s = -\ln R_o$. For that purpose, observe that for $s \to \infty$ equations (2.21)–(2.22) have a critical point at $R_o r_1 = 0$, $v = 0$ and, therefore, they can be linearized around that point, simplifying to

$$\frac{\mathrm{d}R_o r_1}{\mathrm{d}s} = \frac{v(1 + 6sR_o r_1)}{s}, \tag{2.24}$$

$$\frac{\mathrm{d}v}{\mathrm{d}s} = -2v - R_o r_1. \tag{2.25}$$

From expansions in inverse powers of $s$ for $R_o r_1$ and $v$, one obtains from (2.24)–(2.25) the asymptotic behaviors for large $s$,

$$R_o r_1 = \frac{1}{6s} + O(1/s^2), \quad v = -\frac{1}{12s} + O(1/s^2), \tag{2.26}$$

which show that the critical point is an attractor. The results (2.26) can be checked with those in figure 2 which represents the trajectories in the $(R_o r_1, v)$-plane resulting from the numerical integration of the reduced system (2.24)–(2.25) for several initial conditions. We have also performed numerical calculations (not shown here) for the complete system (2.21)–(2.22) and checked that the critical point is indeed a global attractor if $R_o r_1 > 0$. It can be seen that, independently of the initial values of $s$, $R_o r_1 > 0$ and $v$, the system approaches the asymptotic values (2.26). However, the speed of convergence strongly depends on the initial values. In fact, as depicted in figure 3($a$), for some initial conditions the trajectories approach the attractor for values of $s$ so large that the corresponding $R_o = \exp(-s)$ are so small that these could never be observed in practice; only if the initial conditions are appropriate do the solutions converge rapidly to their asymptotic values and may be observable. Note also from figure 2 the important fact that if the initial value of the curvature is negative ($R_o r_1 < 0$), the absolute value of $R_o r_1 < 0$ grows larger with $s$, and eventually breakup will not be slender. Therefore, slender breakup can only be achieved for positive values of $R_o r_1$, while perturbations of the interface for which $R_o$ is a local maximum will amplify and the breakup will not remain slender. On the other hand, linearization of (2.20) near the attractor yields

$$\frac{\mathrm{d}\ln p}{\mathrm{d}s} = -\frac{1/2 - sR_o r_1 - 2sv}{s} \tag{2.27}$$

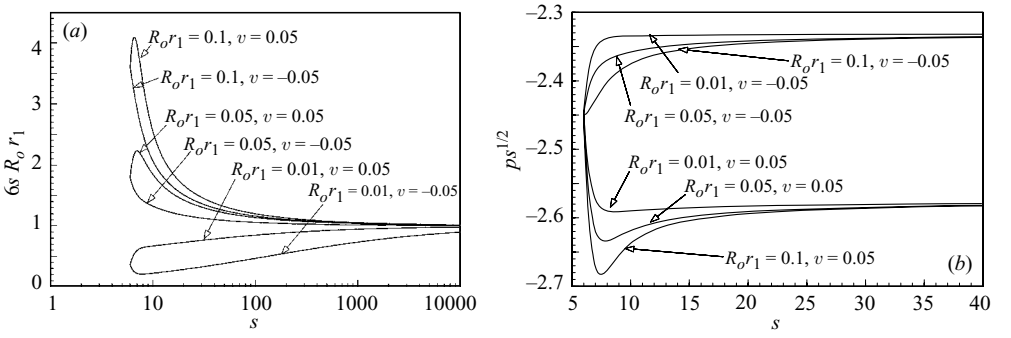


FIGURE 3. Dependence of (*a*) $R_o r_1$ and (*b*) $p$ on $s$ for several initial conditions: $s_0 = 6$, $p = -1$, and the initial values for $v$ and $R_o r_1$ are indicated in the figure. Note that, independently of the initial conditions, both $R_o r_1$ and $p$ tend to their asymptotic values, but with a different rate of convergence. More precisely, $R_o r_1$ tends to its asymptotic value faster the larger its initial value, while the opposite trend is observed for $p$. This result is consistent with the fact that the smaller the values of $R_o r_1$, the more closely the free surface approaches a cylinder.

and, since $sR_o r_1 + 2sv \sim O(1/s) \ll 1/2$ (see (2.26)), equation (2.27) can be readily integrated provided at leading order

$$p\sqrt{s} = K_1 + O(1/s). \tag{2.28}$$

As depicted in figure 3(*b*), $p\sqrt{s}$ tends to a constant for sufficiently large values of $s$, confirming the result in (2.28). By using equation (2.19) defining $p$,

$$\frac{\mathrm{d}R_o^2}{\mathrm{d}t} = \frac{2\sqrt{2}K_1}{\sqrt{-\ln R_o^2}} \rightarrow \int_{R_o^2}^{0} \sqrt{-\ln R_o^2}\,\mathrm{d}R_o^2 = 2\sqrt{2}K_1(t_b - t). \tag{2.29}$$

On integration by parts one obtains

$$-R_o^2\sqrt{-\ln R_o^2} + \frac{1}{2}\int_{R_o^2}^{0} \frac{\mathrm{d}R_o^2}{\sqrt{-\ln R_o^2}} = 2\sqrt{2}K_1\tau \rightarrow \tau = K_2 R_o^2\sqrt{-\ln R_o^2} + O\left(1/\ln R_o^2\right), \tag{2.30}$$

which is the result found in Gordillo *et al.* (2005). Also observe in figure 3(*b*) that the asymptotic limit, $\tau \propto R_o^2\sqrt{-\log R_o^2}$, is reached at a length scale which is smaller the larger is the initial curvature of the interface ($r_1$). Consequently, the asymptotic limit will be easily measurable in those cases in which the initial shape of the bubble surface is sufficiently slender or, equivalently, if $r_1$ is initially small. This explains why the asymptotic solution is easily reached for the limit of large Froude numbers in Bergmann *et al.* (2006). When the initial curvature of the interface is large, the asymptotic limit can only be reached for such small length scales that it would be difficult to measure experimentally (see the case $R_o r_1 = 0.1$ in figure 3*b*). In these situations, different time evolutions with exponents larger than 1/2 will be observed depending on the initial conditions and, consequently, the discrepancies of some experiments with respect to the analytical solution may be explained as a consequence of the slow convergence to the asymptotic limit (2.30). This could be interpreted as a lost of universality in bubble pinch-off (Bergmann *et al.* 2006). However, the universal solution (2.30), can always be numerically calculated under the initial assumptions for which the analysis is valid provided that the computation is carried out for sufficiently small values of $R_o$. Moreover, on introducing (2.26) into

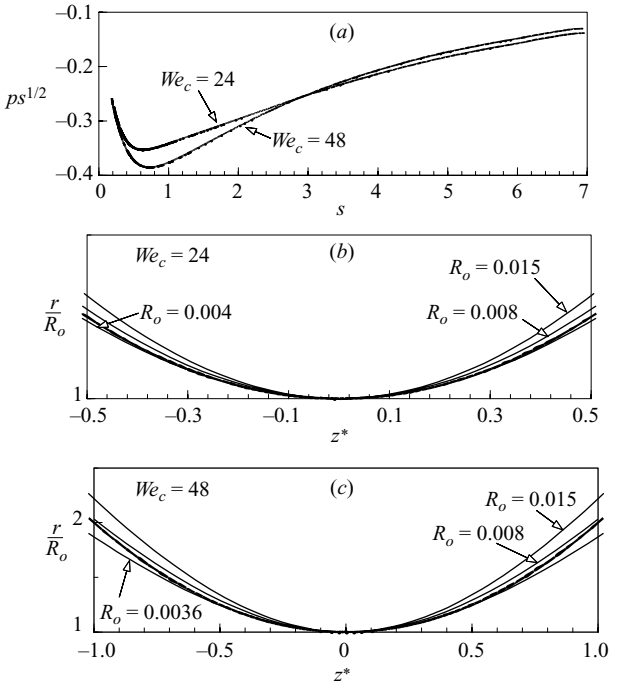


FIGURE 4. Boundary integral numerical simulations with $We_c = 24$ and 48, $\rho_g/\rho = 1.2 \times 10^{-4}$ and 513 nodes. Note that, consistently with the asymptotic results, $p\sqrt{s}$ tend to a constant in ($a$). The local bubble shape in ($b$) and ($c$) approach the analytical solution (2.31), represented with a thick continuous line. $z^* = z/(R_o\sqrt{-6\ln R_o})$.

(2.5), one obtains the shape of the interface near the minimum for sufficiently large values of $s$, namely

$$f(z,t) = R_o\left[1 - \frac{1}{6\ln R_o}\left(\frac{z}{R_o}\right)^2\right]. \tag{2.31}$$

In figure 4 we show numerical simulations obtained with the boundary integral code described in Rodríguez-Rodríguez *et al.* (2006). The bubble centre is initially placed at $r = 0, z = 0$ within an axisymmetric straining flow whose potential at infinity is given by $\phi_\infty = -(1/8)r^2 + (1/4)z^2$; the density ratio between the inner to outer fluids is $1.2 \times 10^{-4}$, and $We_c = 24$ or 48. For more details on the numerical integration, the interested reader is referred to Rodríguez-Rodríguez *et al.* (2006). Consistently with the previous analysis, it is shown in figure 4($a$) that $\mathrm{d}(ps^{1/2})/\mathrm{d}s$ decreases monotonically with $s$. Moreover, $\mathrm{d}(ps^{1/2})/\mathrm{d}s < 2 \times 10^{-2}$ at $s = 6$; consequently, $p\sqrt{s}$ tends to a constant. Figure 4($b$, $c$), in which $z^* = z/(R_o\sqrt{-6\ln R_o})$, also shows that the bubble free surface approaches its universal shape (2.31) for sufficiently large values of $s$.

## 3. Conclusions

We have found an analytical asymptotic solution for the final stages before pinch-off of slender axisymmetric bubbles. Our results reproduce the asymptotic time evolution for the minimum radius, $R_o(t)$, found in Gordillo *et al.* (2005) ($\tau \propto R_o^2\sqrt{-\log R_o^2}$) and

also show that the interface is locally described, for times sufficiently close to pinch-off, by $f(z,t)/R_o(t) = 1 - (6 \ln R_o)^{-1}(z/R_o)^2$, which is in good agreement with existing potential flow numerical simulations of the bubble breakup process. However, we also find that in general these universal, asymptotic solutions are reached extremely slowly, for times so close to pinch-off that they may be difficult to observe, either numerically or experimentally. Most importantly, bubble pinch-off cannot be considered universal from an experimental point of view. Indeed, the time evolution of the bubble interface strongly depends on the initial value of the Reynolds number: if $Re_c$ is sufficiently small, the time evolution of the minimum radius near the singularity will be linear, as described in Doshi *et al.* (2003) and Burton *et al.* (2005). At high values of $Re_c$, the dynamics near the singularity of axisymmetric bubbles depends on whether gas inertia becomes of the order of the liquid inertia at a measurable length scale or not (Gordillo *et al.* 2005). In addition, any asymmetry in the boundary conditions or in the flow can lead to bubble breakup being non-axisymmetric (Neim *et al.* 2005). But, even under the restrictions imposed by assuming large values of $Re_c$, axisymmetry and negligible gas inertia, the time evolution of the bubble interface close to pinch-off strongly depends on initial conditions. If one starts the numerical integration with an interface of large positive curvature ($r_1 > 0$), the asymptotic analytical solutions (2.30)–(2.31) are numerically reached only for extremely small values of the minimum radius, $R_o$. Therefore, these solutions might not be experimentally measured due to a number of reasons such as: experimental limitations, the unavoidable effect of gas inertia, viscosity, the growth of axisymmetric perturbations with a negative radius of curvature, the growth of asymmetric perturbations, or the failure of the continuum approach.

The authors wish to thank D. Lohse and D. van der Meer for providing us with a copy of their submitted manuscript and A. Sevilla, J. Rodríguez-Rodríguez, C. Martínez-Bazán and F.J. Higuera for fruitful discussions. J.M.G. thanks very much Mar's patience during the development of this work. This research has been supported by the Spanish Ministry of Education and Science under Project No. DPI2005-08654-C04-02.

## REFERENCES

Bergmann, R., Meer, D., Stijnman, M., Sandtke, M., Prosperetti, A. & Lohse, D. 2006 Giant bubble pinchoff. *Phys. Rev. Lett.* **96**, 154505.

Burton, J., Waldrep, R. & Taborek, P. 2005 Scaling instabilities in bubble pinch-off. *Phys. Rev. Lett.* **94**, 184502.

Chen, A. U., Notz, P. K. & Basaran, O. A. 2002 Computational and experimental analysis of pinch-off and scaling. *Phys. Rev Lett.* **88**, 174501.

Chen, Y. J. & Steen, P. H. 1997 Dynamics of inviscid capillary breakup: collapse and pinchoff of a film bridge. *J. Fluid Mech.* **341**, 245–267.

Day, R. F., Hinch, E. J. & Lister, J. R. 1998 Self-similar capillary pinchoff of an inviscid fluid. *Phys. Revi. Lett.* **80**, 704–707.

Doshi, P., Cohen, I., Zhang, W. W., Siegel, M., Howell, P., Basaran, O. A. & Nagel, S. 2003 Persistence of memory in drop breakup: The breakdown of universality. *Science* **302**, 1185–1888.

Eggers, J. 1993 Universal pinching of 3D axisymmetric free-surface flow. *Phys. Rev. Lett.* **71**, 3458.

Gordillo, J. M., Sevilla, A., Rodríguez-Rodríguez, J. & Martínez-Bazán, C. 2005 Axisymmetric bubble pinch-off at high Reynolds numbers. *Phys. Rev. Lett.* **95**, 194501.

Leppinen, D. & Lister, J. R. 2003 Capillary pinch-off in inviscid fluids. *Phys. Fluids* **15**, 568–578.

Leppinen, D., Lister, J. & Eggers, J. 2005 Capillary pinch-off of inviscid fluids at varying density ratios: the bubble limit. *Bull. Am. Phys. Soc.* **50**, 9, 63.

Longuet-Higgins, M. S., Kerman, B. R. & Lunde, K. 1991 The release of air bubbles from an underwater nozzle. *J. Fluid Mech.* **230**, 365–390.

Neim, N. C., Moller, P., Zhang, W. W. & Nagel, S. 2005 Bubble pinch-off by inertial collapse: loss of radial symmetry. *Bull. Am. Phys. Soc.* **50**, 9 64.

Oguz, H. N. & Prosperetti, A. 1993 Dynamics of bubble growth and detachment from a needle. *J. Fluid Mech.* **257**, 111–145.

Revuelta, A., Rodriguez-Rodriguez, J. & Martinez-Bazan, C. 2006 Bubble break-up in a straining flow at finite reynolds numbers. *J. Fluid Mech.* **551**, 175–184.

Rodríguez-Rodríguez, J., Gordillo, J. M. & Martínez-Bazán, C. 2006 Breakup time and morphology of drops and bubbles in a high Reynolds number flow. *J. Fluid Mech.* **548**, 69–86.

Suryo, R., Doshi, P. & Basaran, O. A. 2004 Non-self-similar, linear dynamics during pinch-off of a hollow annular jet. *Phys. Fluids* **16**, 4177–4184.